XIII International Conference on Computational Plasticity. Fundamentals and Applications
COMPLAS XIII
E. Oñate, D.R.J. Owen, D. Peric & M. Chiumenti (Eds)

INTEGRATION OF ELASTO-PLASTIC CONSTITUTIVE MODELS IN FINITE DEFORMATION: AN EXPLICIT APPROACH

LLUÍS MONFORTE*, MARCOS ARROYO*, ANTONIO GENS* AND JOSEP M. CARBONELL†

* Departament d'Enginyeria del Terreny, Universitat Politècnica de Catalunya
Jordi Girona 1-3, Campus Nord UPC, 08034 Barcelona, Spain
e-mail: lluismonforte@gmail.com, {marcos.arroyo,antonio.gens}@upc.edu
web page: http://www.etcg.upc.edu

†International Center for Numerical Methods in Engineering (CIMNE)
Gran Capità s/n, Edifici C1, 08034 Barcelona, Spain
e-mail: cpuigbo@cimne.upc.edu, web page: http://www.cimne.com/

Key words: Integration algorithm, finite deformation, elasto-plastic constitutive models

Abstract. This paper highlights an explicit integration scheme for hyperelastic-based finite strains elasto-plastic models. One step update equations are obtained from the large deformation multiplicative elasto-plastic theory, where an exponential variation of the plastic deformation gradient is assumed. The material tangent matrix has the same formal structure as the usual small strains elasto-plastic tangent matrix. The basic algorithm to perform the stress integration, including an adaptive substepping scheme and a yield violation drift correction scheme, are also described. The accuracy and robustness of the proposal is assessed against several examples of typical geotechnical tests. Results from a convergence test suggest that, using an adaptive substepping scheme, the error of the local problem is independent of the step size.

1 INTRODUCTION

The robustness and accuracy of mechanical finite element analysis relies on the local integration scheme of the constitutive equations. In the literature, two main families of schemes have been proposed for large deformation elasto-plastic analysis [1].

The first one is based on an additive decomposition of the plastic and elastic strains and the use of an hypoelastic rate constitutive model. This kind of schemes are extensions of the usual small strains and additional terms are added in order to deal with the rigid body rotation and ensure the objectivity of the resulting stress increment [2, 3]. Because of this, such formulations are restricted to small strains and large displacements [4].

In the second family, a multiplicative decomposition of the deformation gradient along with an hyperelastic response are assumed; stresses are integrated implicitly in time, leading to the

return mapping algorithms [5, 6, 7]. Usually, the Hencky strain measure is introduced and the obtained equations preserve the form of the small strains counterpart.

Altough implicit methods render second order convergence rate of the global problem [8], strong non-linear features of complex plastic models, such as high curvature of the yield surface, may lead to a lack of convergence of the local problem for a range of initial trial states [9].

In this work, an explicit integration scheme for multiplicative finite-strains elasto-plasticity is presented. The equations to perform a single-step elasto-plastic update are presented, where and hyperelastic model and an exponential variation of the deformation gradient are assumed. Since the obtained scheme is first order in time, an automatic substepping technique with error control is used to increase the accuracy [10]. Finally, a set of numerical test are performed to assess using the Houlsby hyperelastic model [11] along with the Modified Cam Clay.

2 ONE STEP ELASTO-PLASTIC UPDATE

Large deformation elasto-plastic analysis are based on a multiplicative split of the deformation gradient, F, in an elastic and plastic part. That is, an intermediate configuration of irreversible (plastic) deformations is introduced, relative to which the elastic response of the material is characterized. As a consequence, the local problem (that is, the strain decomposition, the elastic model, the yield criterion, the hardening law and the flow rule) is defined with the following expressions and the Kuhn-Tucker conditions [5]:

$$F = \frac{\partial \varphi(X,t)}{\partial X} = F^e \cdot F^p \tag{1}$$

$$\tau = 2F^e \cdot F^{eT} \cdot \frac{\partial \bar{W}}{\partial (F^e \cdot F^{eT})} = W(F^e \cdot F^{eT}) \tag{2}$$

$$\Psi(\tau, h) \leq 0 \tag{3}$$

$$h = h(F^p \cdot F^{pT}) \tag{4}$$

$$l^p = \gamma \partial_\tau G(\tau, q) \tag{5}$$

where φ is the motion of the continuum body, where τ is the Kirchhoff stress, $\bar{W}$ is the stored-energy function, Ψ is the yield criterion function, h represent the hardening parameters, G is the plastic potential, γ is the plastic multiplier and l^p is the plastic velocity gradient defined in the final configuration.

The temporal variation of the plastic deformation gradient may be obtained as $\dot{F}^p = \bar{L}^p \cdot F^p$, where $\bar{L}^p$ is the plastic velocity gradient defined in the intermediate configuration. Assuming that the variation of the plastic deformation gradient is exponential [5], the following explicit approximation is obtained:

$$F^p_{n+1} = \exp(\Delta t \bar{L}^p_n) \cdot F^p_n \tag{6}$$

Introducing this equation to the definition of the deformation gradient, equation (1), at time $n+1$:

$$F_{n+1} = F^e_{n+1} \cdot \exp(\Delta t F^{e-1}_n \cdot l^p_n \cdot F^e_n) \cdot F^p_n \tag{7}$$

where the relation $l^p = F^e \cdot \bar{L}^p \cdot F^{e-1}$ has been introduced.

Then, the following expression for the elastic Left Cauchy-Green tensor, the variable governing the elastic response, is obtained:

$$b^e_{n+1} = F^e_{n+1} \cdot F^{eT}_{n+1} = f^{n+1}_n \cdot \exp(-\Delta\gamma\partial_\tau G_n) \cdot \cdot b^e_n \cdot \exp(-\Delta\gamma\partial_\tau G_n)^T \cdot f^{n+1T}_n \tag{8}$$

where $f^{n+1}_n = F_{n+1} \cdot F^{-1}_n$ is the relative deformation gradient.

Note that equation (8) defines the new elastic configuration in terms of quantities in the previous configuration, the new deformation gradient, F_{n+1}, which is obtained in the global problem, and the plastic multiplier.

In implicit methods, a similar expression to equation (8) is obtained. In that case, the Hencky strain measure, $\epsilon = 1/2\ln(b)$, is usually introduced and the obtained equations preserve the form of the small strains schemes [6, 7, 12]. This is not the case of explicit methods: the relative deformation gradient does not commute (in general) with the rest of the terms of the right hand side; as a consequence, the logarithm of the right hand side is not equal to the sum of the logarithm of each term.

The value of the plastic multiplier is obtained from the consistency condition:

$$\Delta\gamma = \frac{\frac{\partial\Psi}{\partial\tau} \cdot D_e \cdot \nabla\delta u}{H + \frac{\partial\Psi}{\partial\tau} \cdot D_e \cdot \frac{\partial G}{\partial\tau}} \tag{9}$$

where the plastic modulus is $H = -\frac{\partial\Psi}{\partial h} \cdot \frac{\partial h}{\partial\epsilon_p} \cdot \frac{\partial G}{\partial\tau}$.

The constitutive tangent matrix may be defined as:

$$\delta\tau = \left[D_e - \frac{D_e \cdot \partial_\tau G \otimes \partial_\tau\Psi \cdot D_e}{H + \partial_\tau\Psi \cdot D_e \cdot \partial_\tau G} \right] \nabla\delta u \tag{10}$$

This matrix has the same formal structure as the usual small strains tangent matrix. In the development of the equations some approximations have been made in the plastic multiplier and the tangent matrix; this fact does not affect the accuracy of the algorithm since the strain update, equation (8), remains unchanged; however, it may slightly deteriorate the convergence rate of the global problem and produce some yield surface drift.

In purely elastic regime, $\Delta\gamma = 0$, the proposal reduces to the usual large deformation elastic update equations, $b^e_{n+1} = f^{n+1}_n \cdot b^e_n \cdot f^{n+1T}_n$ and $\bar{b}^p_{n+1} = \bar{b}^p_n$. As a consequence, the increment of deformation is computed analytically.

3 GAUSS POINT ALGORITHM

The general scheme that is used to integrate the elasto-plastic equations is detailed in Algorithm 1 and is based on Sloan et al [10].

First, a trial elastic state is computed; if the final stress state lays inside the elastic region, deformation occurs in purely elastic regime. In this case the increment of the deformation is computed analytically and no special treatment of the non-linearity of the elastic moduli is required in hyperelastic models.

Otherwise, part or all of the deformation increment produce plastic deformation. Two flags control if there exist elastic loading or elastic unloading before the plastic flow. In both cases, first the yield surface intersection is found using the bisection method and having in mind that the relative deformation gradient may be subidivied as:

$$f_{n+\epsilon}^{n+\theta} = \left(\theta f_n^{n+1} + (1-\theta)1\right) \cdot \left(\epsilon f_n^{n+1} + (1-\epsilon)1\right)^{-1} \tag{11}$$

Then, the rest of the deformation increment is integrated using the elasto-plastic relations.

Elasto-plastic equations are integrated using an adaptive substepping scheme. Each deformation increment is computed with two different temporal discretizations; at the end of the step two stress approximations are obtained: τ and τ^*. Then, the following error measure is defined:

$$R = \frac{\|\tau - \tau^*\|}{\|\tau^*\|} \tag{12}$$

Only in the case that the error measure is lesser than a specified tolerance, Tol_τ, the obtained state is accepted; otherwise is rejected. In both cases, the new pseudo-time increment is computed according to:

$$\Delta\alpha^{new} = 0.9 \left(\frac{\text{Tol}_\tau}{R}\right)^{0.5} \Delta\alpha^{old} \tag{13}$$

For practical reasons, a minimum step-size is also defined to prevent very small increments; as a consequence, increments that do not fulfill the tolerance are sometimes accepted.

Using explicit integration schemes, at the end of each elasto-plastic increment, the obtained stresses typically do not lay in the yield surface. Even using a substepping scheme, the yield surface drift violation may not be negligible and its effects are accumulative [10].

In this work, stresses and hardening parameters are corrected such that the total strains (that is, the deformation gradient) remain unchanged. Performing a Taylor's series of the yield surface function, the following expression is obtained for the plastic multiplier:

$$\Delta\gamma = \frac{\Psi_0}{H + \partial_\tau \Psi \cdot D_e \cdot \partial_\tau G} \tag{14}$$

where Ψ_0 is the yield surface drift violation.

This value is introduced to equation (8) and the incremental deformation gradient is set equal to the identity. This process is iterated until a convergence criterion is fulfilled.

4 EXAMPLES

In this section, first the equations describing the Modified Cam Clay elasto-plastic model are briefly described; the interested reader is referred to [12, 6] for further information. Then, a set of numerical examples are presented.

Algorithm 1: Stress integration with error control (Based on Sloan et al [10])

Data: b^e_n, h_n, f^{n+1}_n
$\Psi^0 = \Psi(\tau_n, h_n)$; $\tau^{tr}_{n+1} = W(f^{n+1}_n \cdot b^e_n \cdot f^{n+1T}_n)$; $\Psi^{tr} = \Psi(\tau^{tr}_{n+1}, h_n)$;
if $\Psi^{tr} < TOL$ **then**
  $b^e_{n+1} = f^{n+1}_n \cdot b^e_n \cdot f^{n+1T}_n$; $h_{n+1} = h_n$; % Elastic step
else
  Flag$_1$ = ($\Psi^0 < -\text{Tol}_f$ and $\Psi^{tr} > \text{Tol}_f$) % Elastic loading + plastic flow
  Flag$_2$ = $\left(\frac{\partial_\tau \Psi \cdot D_e \cdot \delta\epsilon}{\|\partial_\tau \Psi\| \|D_e \cdot \delta\epsilon\|} < \text{Tol}_L\right)$ % Elastic unloading + plastic flow
  if *(Flag$_1$ or Flag$_2$)* **then**
    Find α such that $\Psi(W(b^e_{n+\alpha}), h_n) = 0$; % Yield surface intersection
    where $b^e_{n+\alpha} = f^{n+\alpha}_n b^e_n f^{n+\alpha T}_n$
    Set $h_{n+\alpha} = h_n$
  else
    $\alpha = 0$
  end
  while $\alpha < 1$ **do**
    Integrate elasto-plastic equations with substepping and error control
  end
  Perform Drift Correction
end
$\tau_{n+1} = W(b^e_{n+1})$
Result: $b^e_{n+1}, h_{n+1}, \tau_{n+1}$

4.1 Modified Cam Clay model

The elastic response is characterized by the Houlsby [11] free energy potential:

$$\bar{W}(\epsilon^e) = p_r k^* \exp(\frac{-\epsilon^e_v}{k^*})(1 + \frac{\alpha}{k^*}\|\epsilon^e_d\|^2) \tag{15}$$

Then, the volumetric and deviatoric Kirchhoff stresses, $\tau = p1 + \tau_d$, are computed according to:

$$p = p_r \exp(\frac{-\epsilon^e_v}{k^*})(1 + \frac{\alpha}{k^*}\|\epsilon^e_d\|^2) \tag{16}$$

$$\tau_d = 2\alpha p_r \exp(\frac{-\epsilon^e_v}{\kappa^*})\epsilon^e_d \tag{17}$$

From the previous equations it can be seen that both the bulk and the shear moduli depend on the mean pressure. The bulk modulus also varies with the distortional strain; the Poisson ratio is variable and not directly imposed.

The problem is completed with the yield surface and the hardening law:

$$\Psi(\tau, p_c) = (q/M)^2 + p(p - p_c) \tag{18}$$

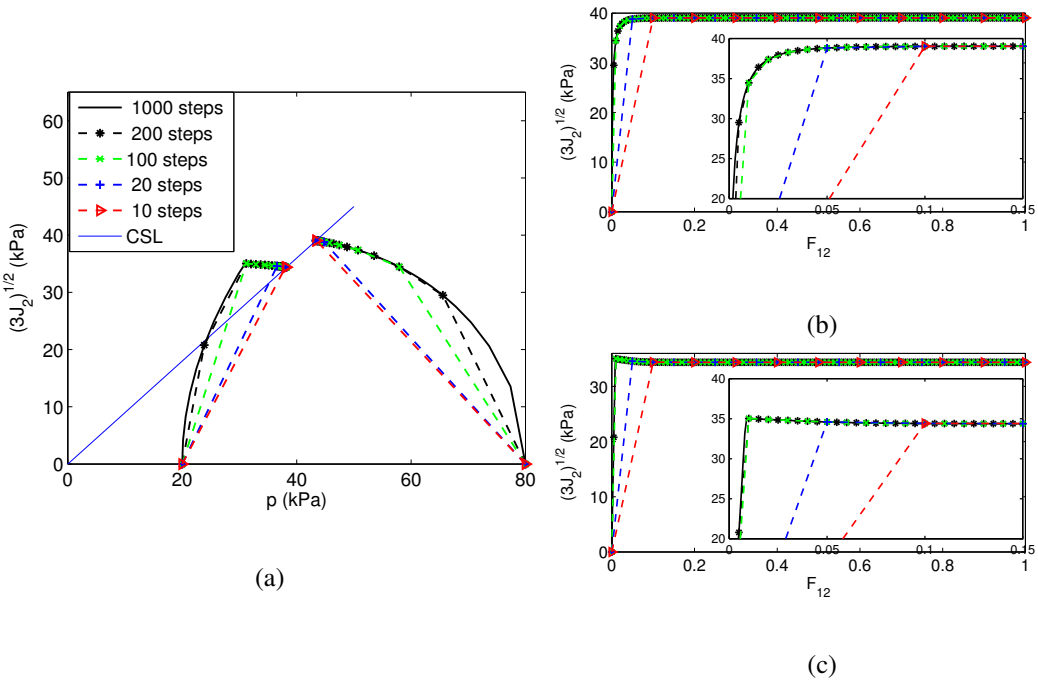

(a)

(b)

(c)

Figure 1: Constant volume shear test: (a) stress trajectories for OCR $= 1$ and 4; stress-strain relations for the normally consolidated (b) and overconsolidated (c) tests.

$$p_c = p_{c0} \exp\left(\frac{-\epsilon_v^p}{\lambda^* - \kappa^*}\right) \tag{19}$$

where $q = \sqrt{3J_2}$,

The chosen soil parameters are: $\kappa^* = 0.0078$, $\lambda^* = 0.085$, $\alpha = 120$, $M = 0.9$ and $p_{c0} = 80$ kPa. p_r is equal to 80 kPa for normally consolidated tests and 20 kPa for overconsolidated tests. In the numerical examples, all the tolerances -in the relative stress error, the yield surface violation and the unloading condition- are set equal to 10^{-5}

4.2 Constant Volume Simple Shear Test

The first example consists on a constant volume simple shear test. The problem is integrated with several number of steps up to a final deformation of $F_{12} = 1.0$. The displacement field is parametrized by a pseudotime variables, t, and is written as: $u(x, y, z, t) = (yt, 0, 0)$; as a consequence, the deformation gradient is:

$$F = \begin{pmatrix} 1 & t & 0 \\ 0 & 1 & 0 \\ 0 & 0 & 1 \end{pmatrix} \tag{20}$$

Figure 1(a) shows the stress trajectory for two overconsolidation ratios; both tests tend to the critical state line. As it can be seen in the overconslidated test, in the elastic regime there exist a change in the mean stress at a constant volumetric strain due to the coupling in the non-linear elastic model. The stress-strain relation is depicted in Figures 1(b) and 1(c); while the

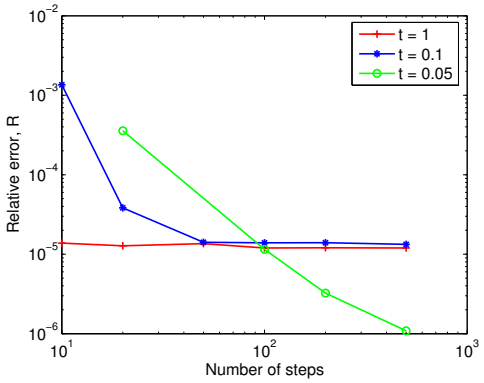

Figure 2: Constant volume shear test: Stress relative error (with respect to the solution obtained with a larger number of steps) for the normally consolidated test at different pseudotimes

normally consolidated test is characterized by a decrease on the stiffness in the plastic regime, the overconsolidated counterpart exhibits softening. The obtained results are in agreement with those reported in [6] using an implicit technique.

In both cases, the solution computed with a small number of steps converges towards that obtained with a larger resolution. As depicted in Figure 2, for a large number of steps the relative error on the stress is in the same order of the tolerance specified at the substepping scheme (10^{-5}). However, when the solution is computed with a small number of increments, larger errors are encountered: the substepping scheme computes several increments with the imposed minimal increment size without converging, thus introducing error to the solution.

In all cases the yield surface drift violation is small and less than three iterations are required to perform the correction.

4.3 Drained triaxial

The last example corresponds to a drained triaxial of a sample of 4×1.6; the initial and final axisymmetric mesh is displayed in Figure 3(d). The initial state of the soil is characterized by $p = 80$ kPa and $q = 0$. A total 1400 steps are computed applying a vertical displacement of $-2.5 \cdot 10^{-3}$ to the top boundary.

In the stress-invariants space, the test tends towards the Critical State Line $q = Mp$, Figure 3(a). Due to the variable Poisson's ratio, this line presents a slight curvature. Figure 3(c) shows the volumetric behavior along with the Normal Compression Line and the Critical State Line. From the model definition, equations (16) and (19), and asssuming that $p_{c0} = p_r$, the following expression relating the volumetric strain and the mean stress at critical state may be obtained:

$$p_{CSL} = p_r \exp(-\frac{\epsilon_v - a_d + (\lambda^* - \kappa^*)\ln(2)}{\lambda^*}) \tag{21}$$

where $a_d = \kappa^* \ln(1 + \alpha\|\epsilon_d^e\|^2/\kappa^*)$ appears due to the coupling in the hyperelastic model. Ac-

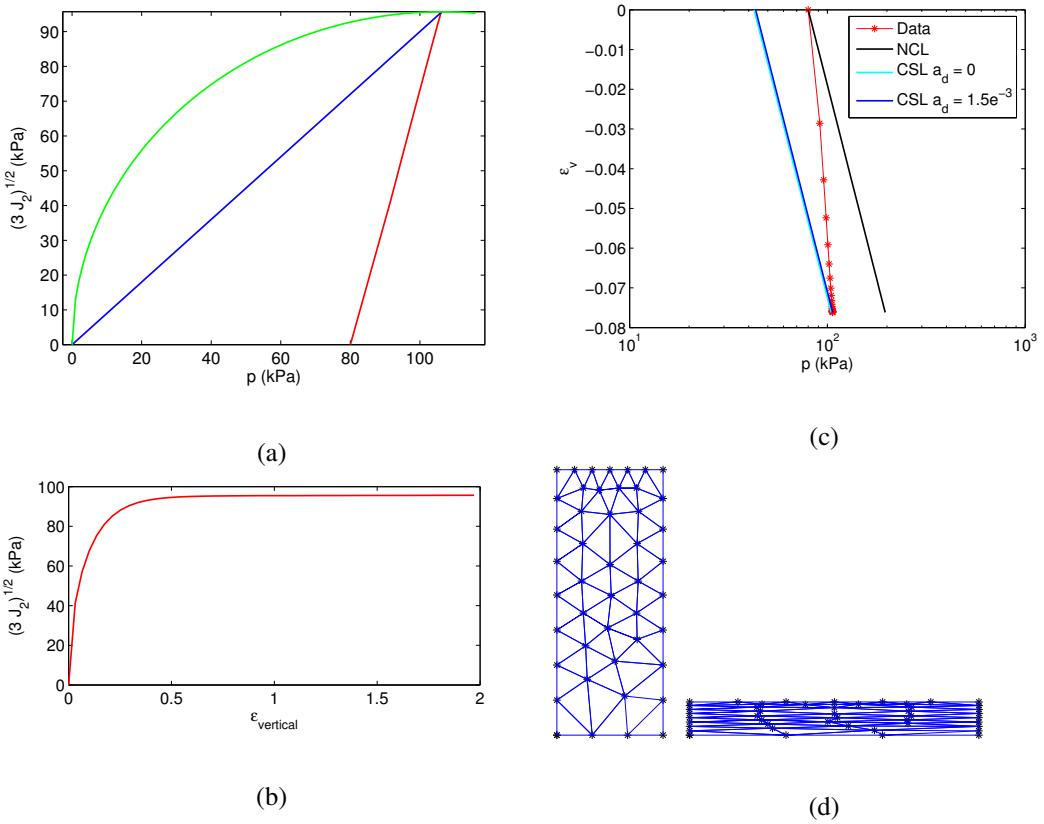

Figure 3: Triaxial test: trajectories in the (a) $p-q$, (b) $\epsilon_{vertical}-q$ and (c) $p-\epsilon_v$ planes; (d) initial and final FEM mesh.

cording to numerical simulations, this term is $a_d = 1.497 \cdot 10^{-3}$. Altough the CSL deppends on the elastic deviatoric deformation; the volumetric (elastic and plastic) and deviatoric elastic deformations cease to increase.

5 CONCLUSIONS

In this work, an explicit integration scheme in the framework of multiplicative finite strains elasto-plasticity has been presented. Routines to alleviate the main drawbacks of explicit methods have been outlined, such as a yield surface drift correction scheme and an adaptive substepping algorithm. By means of several examples using the Houlsby hyperelastic model and the Modified Cam Clay, it has been shown that the obtained results are accurate. Indeed, using an adaptive substepping scheme very similar results are obtained irrespectively of the number of incremental steps; the yield surface drift violation is small and less than three iterations are required to perform the correction.

ACKNOWLEDGMENTS

The support of the Ministry of Education of Spain through research grant BIA2011 - 27217 is gratefully acknowledged.

REFERENCES

[1] Simo, J. C. & Hughes, T. J. R. *Computational Inelasticity*. (1998) New York: Springer.

[2] Nazem, M., Sheng, D. & Carter, J. P. Stress integration and mesh refinement for large deformation in geomechanics. *International Journal for Numerical Methods in Engineering* (2006) 65(7), 1002–1027.

[3] Nazem, M., Carter, J. P., Sheng, D. & Sloan, S. W. Alternative stress-integration schemes for large-deformation problems of solid mechanics. *Finite Elements in Analysis and Design* (2009) 45(12), 934–943.

[4] Bathe, K.-J. *Finite Element Procedures*. (1996) New Jersey: Prentice-Hall.

[5] Simo, J. C. Numerical analysis and simulation of plasticity. In P. Ciarlet and J. Lions (Eds.), *Handbook of Numerical Analysis Vol VI*, (1998) pp. 183 – 499. Elsevier.

[6] Rouainia, M. & Wood, D. M. An implicit constitutive algorithm for finite strain cam-clay elasto-plastic model. *Mechanics of Cohesive-frictional Materials* (2000) 5(6), 469–489.

[7] Armero, F. & Pérez-Foguet, A. On the formulation of closest-point projection algorithms in elastoplasticity – Part I: The variational structure. *International Journal for Numerical Methods in Engineering* (2002) *53*(2), 297–329.

[8] Rouainia, M. & Wood, D. M. Computational aspects in finite strain plasticity analysis of geotechnical materials. *Mechanics Research Communications* (2006) 33(2), 123–133.

[9] Pérez-Foguet, A. & Armero, F. On the formulation of closest-point projection algorithms in elastoplasticity - Part II: Globally convergent schemes. *International Journal for Numerical Methods in Engineering* (2002) 53(2), 331–374.

[10] Sloan, S. W., Abbo, A. J. & Sheng, D. Refined explicit integration of elastoplastic models with automatic error control. *Engineering Computations* (2001) 18(1/2), 121–194.

[11] Houlsby, G. The use of a variable shear modulus in elastic-plastic models for clays. *Computers and Geotechnics* (1985) 1(1), 3–13.

[12] Borja, R. I. & Tamagnini, C. Cam-clay plasticity Part III: Extension of the infinitesimal model to include finite strains. *Computer Methods in Applied Mechanics and Engineering* (1998) 155(1), 73–95.